





Electroconvection of a nematic liquid crystal in polymer networks as porous media

Hiroki Ifuku, Ryohei Kojima , Hirotaka Okabe , Shinya Kawano, Kazuhiro Hara , and Yoshiki Hidaka ^{*}

Department of Applied Quantum Physics and Nuclear Engineering, Faculty of Engineering, Kyushu University, Fukuoka 819-0395, Japan



(Received 30 May 2025; accepted 5 August 2025; published 27 August 2025)

The polymer network liquid crystal (PNLC), in which a polymer network is formed within a nematic liquid crystal, can be regarded as a porous medium. In this study, we discover electroconvection in the PNLC and examine its nonlinear, nonequilibrium physical properties. As the monomer weight fraction increases, distortions in the convective pattern emerge and the temporal fluctuations slow. The polymer network hinders the reorientation of the liquid crystal molecules, thereby suppressing the motion of the convection pattern. Furthermore, measurements of the electric Nusselt number, which characterizes the electrical transport phenomena, reveal that, as the monomer weight fraction increased, the threshold voltage for the onset of convection increased and the efficiency of charge transport decreased. This study quantitatively evaluated the nonlinear, nonequilibrium phenomena of the PNLC as flow phenomena in porous media.

DOI: [10.1103/3cwl-nl1m](https://doi.org/10.1103/3cwl-nl1m)

I. INTRODUCTION

Mixing a liquid crystal with a photoreactive monomer and polymerizing the mixture under ultraviolet irradiation yields a structure in which liquid crystals are embedded in a three-dimensional polymer network. Such polymer network liquid crystals (PNLCs) have attracted attention for their functional properties, leading to extensive applied research. Polymerization of liquid-crystalline monomers preserves the liquid crystal alignment established before polymerization [1]. Utilizing this property, applications such as voltage-controlled smart glass, which can switch between transparent and opaque states have been actively pursued. Furthermore, studies have been conducted to extend the temperature range of the blue phase, which is promising for high-speed display applications, by employing polymer stabilization [2]. While research on the applications of these functional materials has been active, fundamental studies on PNLCs have primarily focused on chemical approaches to equilibrium states. In contrast, Hoischen, Kitzrow *et al.* performed ultraviolet polymerization in a nematic liquid crystal containing a liquid crystalline monomer in which an ordered electroconvection structure had formed, thereby preserving spontaneous pattern formation in a nonequilibrium state and enabling the fabrication of phase gratings and polymer films with periodic surface modulation [3].

Liquid crystals exhibit distinctive nonequilibrium phenomena due to their softness and anisotropy, and under strongly nonequilibrium conditions, a variety of nonlinear phenomena can be observed. Such nonlinear nonequilibrium phenomena are expected to facilitate the development of postdisplay technologies employing liquid crystals. Among these phenomena, nematic electroconvection, which occurs when an electric field is applied to a nematic liquid crystal, is a representative example. In nematic electroconvection, periodic structures in

the flow field spontaneously emerge, analogous to those observed in the Rayleigh-Bénard convection system, where the fluid is heated from below. Accompanying the flow field, a periodic structure in the director field also forms, facilitating pattern observation via optical techniques [4]. Elucidation of the mechanisms underlying the onset of electroconvection and derivation of the threshold voltage and critical wave number through linear stability analysis have been achieved by comprehensively considering the hydrodynamic, elastic, dielectric, and electrical conduction properties of nematic liquid crystals [5]. These studies have significantly advanced the development of liquid crystal physics. Moreover, because nematic electroconvection can be readily induced at relatively low voltages and the resulting patterns are easily observable, it has been widely studied as a model experimental platform for nonlinear nonequilibrium phenomena and convective phenomena.

We discovered that electroconvection occurs in PNLC. In this paper, we treat this phenomenon as convection in porous media and present the results of a detailed investigation into its physical properties.

A porous medium is a material system characterized by many fine voids. Fluid flow phenomena in porous media have traditionally been studied in fields such as geology, as well as in applications such as groundwater flow and oil extraction [6]. A fundamental relation describing fluid flow phenomena in porous media is Darcy's law [7], which expresses the linear relationship between the flow velocity \mathbf{v} and the pressure gradient ∇P , as follows:

$$\mathbf{v} = -\frac{k}{\eta} \nabla P. \quad (1)$$

Here, η denotes the viscosity of the fluid, and k represents the permeability of the porous medium. Among the fluid flow phenomena in porous media, Rayleigh-Bénard convection has long been a prominent topic in physics, and many studies have been conducted on it [8,9]. Studies investigating the influence on ordered convective structures and vertical heat

^{*}Contact author: hidaka.yoshiki.565@m.kyushu-u.ac.jp

transport have been conducted through experiments, theoretical analysis, and numerical simulations [10–15]. For vertical heat transport, measurements and calculations of the Nusselt number, a parameter representing the ratio of convective to conductive heat transport, have been carried out [16,17]. Importantly, polymer networks, whose structures contain numerous fine voids, can be regarded as a type of porous medium. When a pressure gradient is applied to a polymer gel, the velocity of the fluid that seeps out is given by a relation similar to Eq. (1) [18]. In this context, the ratio of the pressure gradient to the flow velocity is measured as a “friction coefficient,” which serves as a parameter characterizing the properties of the polymer gel.

PNLC can be regarded as a system in which a polymer network, acting as a porous medium, contains a liquid crystal as its solvent. Therefore, the electroconvection we discovered in PNLC can be considered a convective phenomenon in porous media. Moreover, to gain a deeper understanding of its physical properties, it is essential to elucidate the dynamic behavior of PNLC under nonequilibrium conditions. Accordingly, by applying research methods from studies of convective phenomena in porous media, we conducted this study to introduce the perspective of nonlinear nonequilibrium properties into PNLC. In the electroconvection of a planar-aligned nematic liquid crystal, various convective patterns emerge depending on the applied voltage [19]. Moreover, the ratio of charge transport by electroconvection to electrical conduction in the absence of convection corresponds to the Nusselt number in Rayleigh-Bénard convection and is referred to as the “electric Nusselt number” [20,21]. In the present study, we quantitatively examine how the electroconvective patterns and the electric Nusselt number in PNLC, considered as a porous medium, are influenced by the polymer network, to deepen our understanding of its nonequilibrium physical properties.

II. EXPERIMENT

In experimental studies of nematic electroconvection, a nematic liquid crystal, *p*-methoxy-benziliden-*p*′-*n*-butylaniline (MBBA), whose conductivity is enhanced by the addition of tetra-*n*-butylammonium bromide (TBAB), is typically used. The increase in conductivity raises the upper frequency limit f_c of the conductive regime in which normal convection occurs. This enables experiments to be conducted in a high-frequency region with minimal adverse effects from charge injection. In this study, MBBA with TBAB at 0.01 wt% was used as the base sample. Following the work of the Kitzerow group [3], we prepared a liquid-crystal sample by mixing the photoreactive monomer RM257 and the photopolymerization initiator Irgacure651 into the base sample to fabricate a PNLC system. To investigate the influence of the polymer network, we prepared liquid-crystal samples with varying weight percentages of RM257 (R [wt%]), as shown in Table I. Generally, increasing the monomer concentration leads to denser polymer networks with smaller voids [22]. In the following, the samples are distinguished according to R [wt%].

In this study, two types of standard planar-aligned nematic liquid-crystal cells with transparent indium-tin-oxide (ITO) electrodes were employed. Hereafter, the rubbing direction is defined as x , and the observation direction as z . In other words,

TABLE I. Samples prepared to investigate the R -dependence.

MBBA + TBAB [wt%]	RM257 (R) [wt%]	Irgacure 651 [wt%]
100	0	0
94	5	1
89	10	1
84	15	1
79	20	1
74	25	1
69	30	1
64	35	1
59	40	1

convective patterns in the x - y plane are observed, and the current in the z direction is measured to determine the electric Nusselt number. Cell I was used for pattern observation; that is, the results in Sec. III A were obtained using this cell. Cell I was prepared by coating an alignment agent and performing rubbing in our laboratory. The electrode dimensions of Cell I are $L_x = 30$ mm and $L_y = 5$ mm. Cell II is used for measuring the electric Nusselt number, that is, the results in Sec. III B were obtained using this cell. For Cell II, we used the “Cells for Use in Testing” from EHC Co., Ltd. The electrode dimensions of Cell II are $L_x = 10$ mm and $L_y = 10$ mm. In both cells, the electrode spacing is 50 μ m.

These liquid crystal cells were filled with the aforementioned liquid-crystal samples. First, the temperature was set to 30.00 ± 0.05 °C using a control system comprising a Kanthal-wire heater, a platinum resistance thermometer, and a proportional-integral-differential regulator. Then, using a UV-LED spot light source (LC-L1V3, Hamamatsu Photonics), the sample was irradiated with ultraviolet light at a wavelength of 365 nm for 15 minutes to form a polymer network. During this ultraviolet irradiation, the light intensity was measured using a UV radiometer (UV-M03A, ORC Manufacturing), and the position and angle of the head unit of the spotlight source were adjusted until the intensity reached 22.3 W/m². Additionally, the head unit was adjusted so that the ultraviolet light strikes the glass plates of the liquid crystal cells perpendicularly. Furthermore, to prevent an increase in the sample temperature due to ultraviolet irradiation, a heat-absorbing filter (Sigma Koki) was installed between the head unit and the liquid crystal cells.

Using the liquid crystal cells fabricated as described above, measurements were conducted in a standard experimental setup for nematic electroconvection. The experimental temperature was also maintained at 30.00 ± 0.05 °C during the measurements. The applied voltage, given by $V_{ac}(t) = \sqrt{2}V \cos(2\pi ft)$, was generated by a synthesizer (WF1946B, NF) that produced a sine wave and was subsequently amplified by an amplifier (9200, Tabor Electronics). The frequency f of the applied voltage is one of the key parameters in nematic electroconvection, as the pattern transition process varies with increasing applied voltage [19]. In this study, a relatively low frequency of $f = 100$ Hz was chosen, which exhibits the standard transition process: Normal Rolls (Williams domain) \rightarrow Defect Turbulence (fluctuating

Williams domain) → Grid Pattern → developed turbulence (Dynamic Scattering Mode; DSM).

We observed the patterns that emerged as the RMS value V of the ac voltage gradually increased. For the observation, a stereomicroscope (SMZ1270, Nikon) and a digital camera (EOS Kiss X8i, Canon) were employed. A stage equipped with an illumination source, a polarizer, and an aperture was integrated into the stereomicroscope, and the liquid crystal cell was mounted on it. Following the standard observation method for planar-aligned nematic electroconvection, a polarizer was installed solely beneath the liquid crystal cell to ensure that the incident light was linearly polarized in the x direction. Initially, $f = 100$ Hz and $V = 5$ V were applied; then, V was increased by 0.05 V every 3 minutes until DSM2 [23] appeared.

Furthermore, to determine the electric Nusselt number, the current flowing through the liquid crystal cell was measured. Since the measured current was a weak ac signal, a lock-in amplifier (5610B, NF) was employed for the measurement. In response to the applied voltage $V_{ac}(t)$, both in-phase and out-of-phase components were extracted [21]. In this study, only the in-phase component $I_r(V)$, which is related to the charge transport in electroconvection, is used as the measured value.

III. RESULTS AND DISCUSSION

A. Pattern transition

To investigate the influence of the polymer network on convective patterns, for each R , the RMS value V of the applied ac voltage was gradually increased while observations were conducted using the stereomicroscope. In the following, the results and discussion for each pattern and the observed phenomena are presented. The captured still images are denoted by $u(x, y)$, and the videos are represented by $u(x, y, t)$. The applied voltage V was gradually increased, and the voltage at which convective patterns appeared in approximately half of the observation area was taken as the convective onset voltage V_c [24]. To compare the differences in convective patterns across different values of R , the applied voltage is expressed in terms of a normalized control parameter

$$\varepsilon = \frac{V^2 - V_c^2}{V_c^2}. \quad (2)$$

In nematic electroconvection, when ε exceeds zero, a stripe pattern known as “Normal Rolls” emerges. Figure 1 shows snapshots of Normal Rolls at $\varepsilon = 0.10$ for different values of R , which illustrate their evolution. Normally, as observed in Fig. 1(a) for $R = 0$, complete stripes are seen; however, for $R \neq 0$, the rolls become distorted, with the distortion becoming more pronounced as R increases.

Figure 2 shows a space-time diagram $u(x, t)$ at a fixed y coordinate, derived from the video $u(x, y, t)$ of Normal Rolls at $\varepsilon = 0.10$. These results indicate that, for $R \neq 0$, the rolls move slowly. Moreover, as R increases, the rolls exhibit more pronounced movement. The distortion of Normal Rolls in Fig. 1 and the motion observed in Fig. 2 resemble the behavior of Defect Turbulence, which arises when the voltage is increased from Normal Rolls, as described later. However, the control parameter $\varepsilon = 0.10$ is too low for Defect

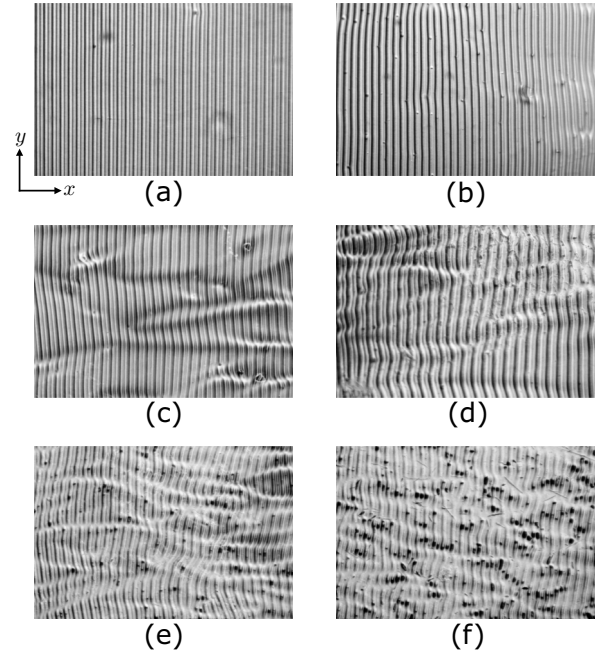


FIG. 1. Image of Normal Rolls at $\varepsilon = 0.10$. Cell I was used. The image size is 2.04 mm in width and 1.36 mm in height. (a) $R = 0$ wt%, (b) $R = 5$ wt%, (c) $R = 10$ wt%, (d) $R = 20$ wt%, (e) $R = 25$ wt%, and (f) $R = 35$ wt%.

Turbulence to occur. Furthermore, in Defect Turbulence, the entire roll pattern fluctuates due to the interaction between convection and molecular alignment in the x - y plane, whereas the motion observed in Fig. 2 is localized, distinguishing it from Defect Turbulence. Therefore, the motion of the Normal Rolls observed in this study is attributed to the influence of the polymer network rather than to Defect Turbulence. Under normal conditions (i.e., when $R = 0$), if disturbances occur in

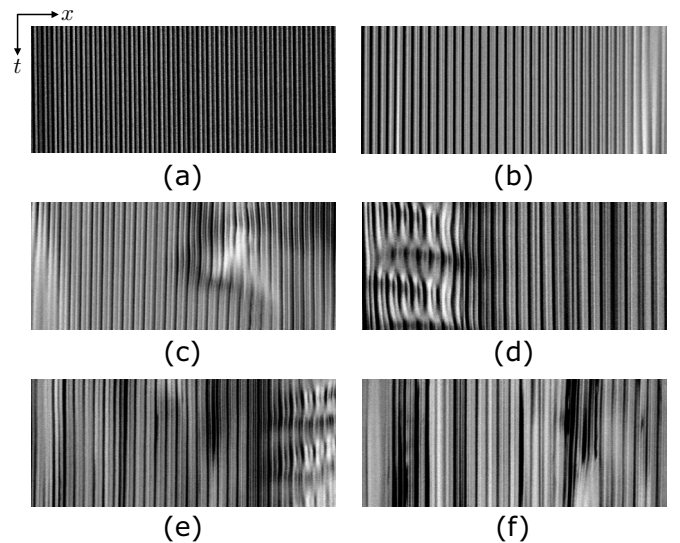


FIG. 2. Space-time diagram of Normal Rolls at $\varepsilon = 0.10$. Cell I was used. The image size is 1.01 mm in width and 400 s in height. (a) $R = 0$ wt%, (b) $R = 5$ wt%, (c) $R = 10$ wt%, (d) $R = 20$ wt%, (e) $R = 25$ wt%, (f) $R = 35$ wt%.

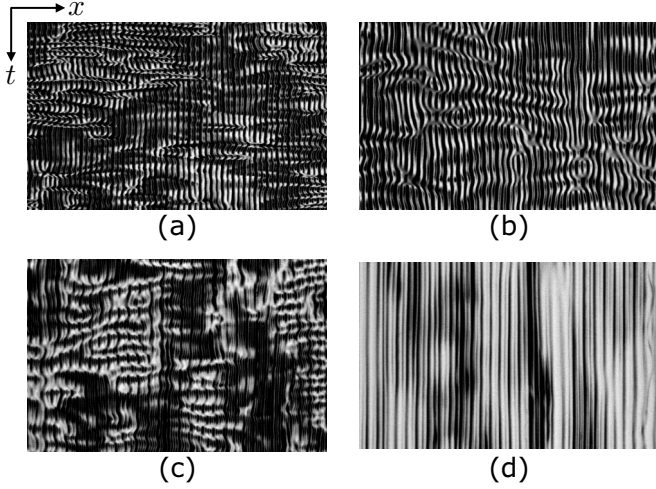


FIG. 3. Space-time diagram of Defect Turbulence at $\varepsilon_{DT} = 0.10$. Cell I was used. The image size is 1.01 mm in width and 600 s in height. (a) $R = 0$ wt%, (b) $R = 15$ wt%, (c) $R = 25$ wt%, (d) $R = 35$ wt%.

the Normal Rolls, they gradually relax over time, eventually leading to a steady state characterized by a complete stripe pattern. However, in the presence of a polymer network, even if disturbances occur in the rolls, the network hinders this relaxation, and the system is thought to remain in a state of continuous fluctuation without reaching a steady state.

In nematic electroconvection, patterns that appear at voltages higher than those for Normal Rolls are generally accompanied by spatiotemporal fluctuations. For PNLCs, we experimentally confirm that as the monomer weight fraction R increases, the characteristic timescale of these fluctuations becomes noticeably longer for every pattern. Accordingly, we focus on Defect Turbulence and show how the fluctuation rate varies with R . Defect Turbulence is generated through the destabilization of Normal Rolls, as described below. When the applied voltage V exceeds a certain threshold, the nematic director in the x - y plane is driven to rotate by a torque arising from viscous anisotropy (the so-called “viscous torque” [25]) induced by the convective flow. This director rotation, in turn, induces a rotation of the convection rolls via the electroconvective effect. The rotation of the convection rolls generates defects within the periodic structure, and these defects glide over a wide range in the x direction. Since the threshold of ε for the onset of Defect Turbulence depends on R , we introduce a new control parameter

$$\varepsilon_{DT} = \frac{V^2 - V_{DT}^2}{V_{DT}^2} \quad (3)$$

based on the threshold voltage for Defect Turbulence, V_{DT} . The applied voltage V was then set so that $\varepsilon_{DT} = 0.10$ for each R , and a video $u(x, y, t)$ was recorded. A space-time diagram $u(x, t)$, obtained using the same method as for Fig. 2, is shown in Fig. 3. Unlike Normal Rolls (Fig. 2), the fluctuations in Defect Turbulence occur uniformly across space. For $R = 0$ [Fig. 3(a)], horizontal streaks that represent the gliding motion of the defects described above are observed. It is evident that as R increases, this gliding motion diminishes. This change is

TABLE II. Relaxation time of fluctuations in Defect Turbulence.

R [wt%]	τ_0 [s]
0	6.6
10	11.9
15	16.1
20	42.8
25	12.2
35	87.2

thought to occur as follows. First, the polymer network hinders changes in the orientation of the liquid crystal molecules. As a result, the fluctuations of the rolls arising from the interaction between alignment and convection are reduced. Consequently, the associated defect motion is also reduced. Furthermore, to quantitatively evaluate the differences in the speed of pattern fluctuations, the correlation time τ_0 for each R is obtained from $u(x, y, t)$ measured at $\varepsilon_{DT} = 0.10$ using the following method. First, the time correlation function averaged over space, $C_{av}(\tau)$, is defined as

$$C(\mathbf{r}, \tau) = \langle [u(\mathbf{r}, t + \tau) - u_0(\mathbf{r})] \cdot [u(\mathbf{r}, t) - u_0(\mathbf{r})] \rangle_t, \quad (4a)$$

$$C_{av}(\tau) = \langle C(\mathbf{r}, \tau) \rangle_{\mathbf{r}}. \quad (4b)$$

Here, $\langle \dots \rangle_*$ denotes an average over $*$, with $\mathbf{r} = (x, y)$ and $u_0(\mathbf{r}) = \langle u(\mathbf{r}, t) \rangle_t$. The average over \mathbf{r} is taken over 190 points arranged in a grid. Except for $R = 5$ wt% and $R = 30$ wt%, $C_{av}(\tau)/C_{av}(0)$ could be well fitted by $\exp(-\tau/\tau_0)$. The τ_0 obtained from this fitting is shown in Table II. From these results, it is found that, except for $R = 25$ wt%, the motion of Defect Turbulence becomes slower as R increases.

Grid Patterns typically appear as isolated islands within turbulence (DSM1), and the area fraction of the grid region exhibits a maximum at a certain applied voltage [26]. Figure 4 shows representative images obtained at this maximum for three selected values of R . The area fraction of the grid region is larger for $R \neq 0$ than for $R = 0$ and reaches its maximum around $R = 10$ – 15 wt% (see Fig. 4). Grid Patterns arise from the freezing of oscillations between the two modes of convective rolls in the turbulent region [26]. Due to the influence of the polymer network, as in Defect Turbulence, these oscillations slow down. As a result, because the lattice freezes more readily, the area fraction of the grid region is considered to increase with R . However, at higher values of R the area fraction decreases again, and many distorted grids appear whose lattice vectors deviate appreciably from the x and y directions [see Fig. 4(c)]. This is also attributed to the influence of the polymer network on the alignment of the liquid crystal molecules, as in the case of Normal Rolls.

In general, as R increases, the transition points between the different patterns become indistinct. One example is the transition between DSM1 and DSM2. In nematic electroconvection, developed turbulence manifests as DSM1 at low applied voltages, where anisotropy resulting from planar alignment persists, and as DSM2 at high applied voltages, where the anisotropy vanishes. Furthermore, because DSM2 scatters light much more strongly than DSM1, the transmitted-light intensity drops markedly [23], and thus allows an unambiguous distinction between the two states.

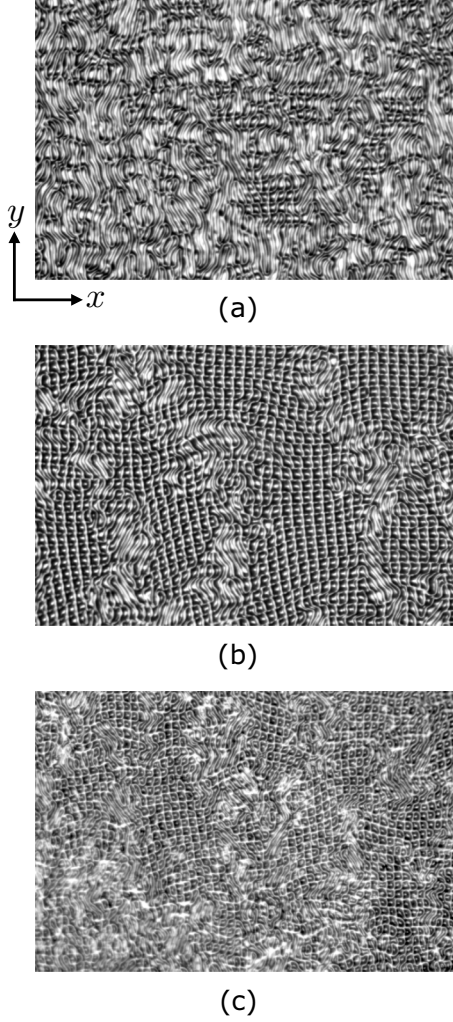


FIG. 4. Images of Grid Pattern obtained with Cell I. The image size is 2.04 mm in width and 1.36 mm in height. (a) $R = 0$ wt%, (b) $R = 15$ wt%, (c) $R = 35$ wt%. For each R the image was taken at the applied voltage at which the area fraction of the grid region reaches its maximum.

Therefore, for $R = 0$ the transition point from DSM1 to DSM2 is well defined; however, as R is increased, the transition, as determined from image intensity, becomes progressively less distinct.

B. Electric Nusselt number

In the region well below V_c , namely, $4.0 \text{ V} \leq V \leq 6.0 \text{ V}$, the measured in-phase component of the current, $I_r(V)$, was well described by a linear function of V . When extrapolated to $V > 6.0 \text{ V}$, this linear function is denoted by $I_{r0}(V)$. At voltages above a certain threshold, a deviation between $I_r(V)$ and $I_{r0}(V)$ is observed [21]. This deviation reflects the charge transport induced by electroconvection. To clearly demonstrate this behavior of the current, the electric Nusselt number

$$\text{Nu}(V) = \frac{I_r(V)}{I_{r0}(V)} \quad (5)$$

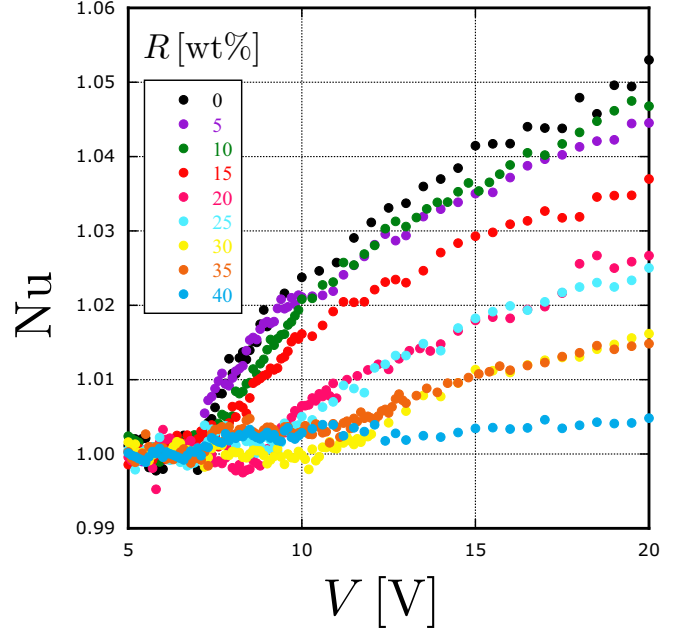


FIG. 5. V -dependence of Nu . The colors represent R [wt%].

is determined. The V dependence of Nu for each R is shown in Fig. 5. For all samples except for $R = 40$ wt%, $\text{Nu} \simeq 1$ for voltages below a certain threshold, above which it begins to increase markedly. This result indicates that charge transport is promoted by convection [21]. The voltage at which the marked increase begins can be regarded as the convective onset voltage V_c . It is found that as R increases, the increase in Nu in the region above V_c becomes more gradual. This is thought to result from the polymer network hindering charge transport by convection. A more gradual increase in the Nusselt number is also observed in Rayleigh-Bénard convection in porous media [10]. Moreover, it can be seen that V_c shifts toward higher voltages as R increases.

As shown in Fig. 6(a), a linear approximation is made for the region where Nu begins to rise, and the voltage at which this line intersects the line $\text{Nu} = 1$ is taken as V_c . However, for samples with $R = 10, 15, 25, 35$ wt%, after an initial slight rise in Nu near the V_c for $R = 0$ (denoted as V_{c0}), a second marked increase is observed. Figure 6(b) shows an enlarged graph for $R = 35$ wt%, where this tendency is most pronounced. For these samples, the voltage at which the second increase occurs was taken as V_c . In this experiment, pattern observations are conducted simultaneously, and V_c is measured by the same method described in Sec. III A. In Fig. 6(c), V_c determined by pattern observation and those determined from Nu are plotted as functions of R . Both sets of V_c increase almost linearly with R . This is also thought to result from the polymer network hindering charge transport by electroconvection. However, the V_c values determined from Nu tended to be smaller than those determined by pattern observation. This is thought to be because the effect of convection in promoting charge transport manifests earlier than the appearance of a convective pattern. For the $R = 40$ wt% sample, no convective pattern is observed even when a considerably high voltage was applied. In this case, Nu exhibited

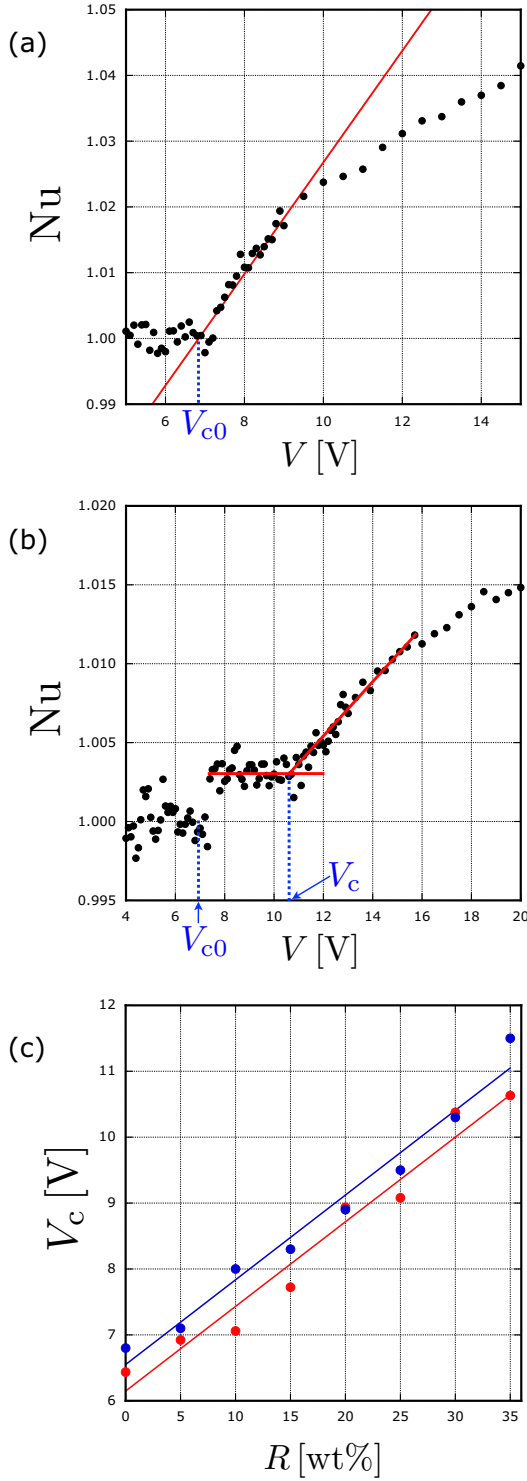


FIG. 6. (a) V dependence of Nu for $R = 0$ wt%. (b) V dependence of Nu for $R = 35$ wt%. (c) R dependence of V_c . The red circles represent V_c determined from Nu by the methods shown in (a) and (b), and the red solid line is the result of a fit given by $V_c(R) = (0.13 \pm 0.01)R + (6.6 \pm 0.2)$. The blue circles represent V_c determined by pattern observation, and the blue solid line is the result of a fit given by $V_c(R) = (0.13 \pm 0.01)R + (6.2 \pm 0.2)$.

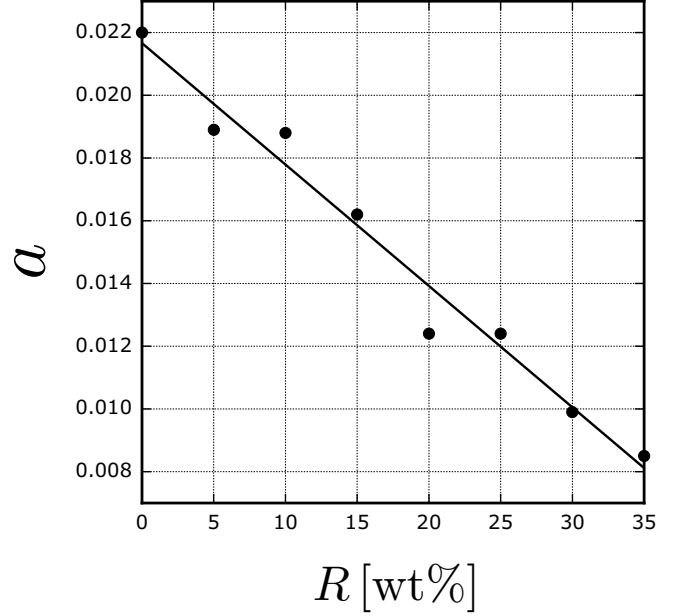


FIG. 7. R dependence of the proportionality coefficient a for $Nu - 1$ with respect to ε . The solid line shows the result of a fit, given by $a(R) = -(3.9 \pm 0.3) \times 10^{-4}R + (0.022 \pm 0.001)$.

only a slight rise near V_{c0} . Since no marked increase is observed, it is impossible to determine V_c . Given the absence of a marked increase in Nu , we infer that not only are the patterns unobservable, but also that convection does not actually occur. In the regime $V > V_{c0}$ for the $R = 40$ wt% sample and in the regime $V_{c0} < V < V_c$ for the samples exhibiting a two-stage increase in Nu , it is considered that although convective flow in the form of circulating motion does not occur, some kind of instability takes place.

To clarify the tendency that as R increases, the rise in Nu beyond V_c becomes more gradual, we focus on the region immediately after Nu begins to rise near V_c in Fig. 5. In this weakly nonlinear region, it was theoretically shown that $Nu - 1 \propto \varepsilon$ [21]. Our experimental results also confirm this linear relationship in the small- ε region, so a linear fit is performed over the region $0 < \varepsilon < 1$ to obtain the proportionality coefficient a . Figure 7 shows that a decreases linearly with R . This result will likely be useful for the theoretical investigation of transport phenomena in PNLC.

IV. CONCLUSION

In electroconvection of polymer network liquid crystals, it was found that the polymer network induced pattern distortion, slowed turbulent fluctuations, increased the convective onset voltage, and reduced electrical transport. In conventional nematic electroconvection (no polymer network), Normal Rolls formed stationary, complete stripes; however, as the monomer weight percentage R increased, distortion in the rolls was observed. At that time, the rolls also exhibited temporal fluctuations that were localized, differing from those in Defect Turbulence. Therefore, the distortion was considered

to arise not from Defect Turbulence, but from the disruption of liquid crystal alignment by the polymer network, and furthermore, the hindrance of the relaxation of this distortion by the polymer network lead to temporal fluctuations. In Defect Turbulence, it was found that as R increases, the glide of defects decreases and the motion of the pattern becomes slower. The convective onset threshold voltage V_c was defined as the voltage at which the electric Nusselt number Nu in nematic electroconvection rises sharply above 1. It was found that V_c increases with increasing R . Furthermore, the rise of Nu above V_c became more gradual as R increased.

In this study, the results were organized according to the experimentally controlled weight percentage R of the monomer RM257. However, the volume fraction ϕ occupied by the polymer network in the system is likely more important. When considering fluid flow in porous media, the relevant porosity is given by $1 - \phi$ [9,27]. If the volumetric change due to the polymerization of RM257 is assumed to be negligibly small, it should be possible to determine the volume fraction of the polymer network using the densities of MBBA, RM257, and Irgacure651. Moreover, a model is proposed that regards the polymer network as a collection of capillaries and considers the fluid flow phenomena within the polymer network to be analogous to Hagen-Poiseuille flow in capillaries [28]. In that case, the volume fraction occupied by the capillaries corresponds to the porosity $1 - \phi$. Further-

more, the capillary diameter corresponds to the mean pore size of a porous medium, and this length scale also influences its flow properties [29,30]. In the PNLC examined in this study, information on the pore size can be obtained by analyzing the network structure in SEM images of the polymer network. Indeed, SEM images have shown that the network morphology varies with the monomer concentration [22]. To discuss electroconvection in PNLCs as porous media in greater detail, such structural observations will be required in future studies.

ACKNOWLEDGMENTS

We wish to thank Dr. Hiroki Higuchi and Prof. Hirotugu Kikuchi for useful information on experimental techniques, and Prof. Heinz-Siegfried Kitzerow for fruitful discussions that inspired this research. This work was supported by JSPS KAKENHI Grant No. 22K03469.

DATA AVAILABILITY

The data that support the findings of this article are not publicly available upon publication because it is not technically feasible and/or the cost of preparing, depositing, and hosting the data would be prohibitive within the terms of this research project. The data are available from the authors upon reasonable request.

-
- [1] I. Dierking, Recent developments in polymer stabilised liquid crystals, *Polym. Chem.* **1**, 1153 (2010).
 - [2] H. Kikuchi, M. Yokota, Y. Hisakado, H. Yang, and T. Kajiyama, Polymer-stabilized liquid crystal blue phases, *Nat. Mater.* **1**, 64 (2002).
 - [3] A. Hoischen, S. A. Benning, and H.-S. Kitzerow, Electroconvection of liquid crystals: Tool for fabricating modulated polymer surfaces, *J. Appl. Phys.* **105**, 013540 (2009).
 - [4] N. Éber, P. Salamon, and Á. Buka, Electrically induced patterns in nematics and how to avoid them, *Liq. Cryst. Rev.* **4**, 101 (2016).
 - [5] E. Bodenschatz, W. Zimmermann, and L. Kramer, On electrically driven pattern-forming instabilities in planar nematics, *J. Phys. France* **49**, 1875 (1988).
 - [6] M. Muskat and R. D. Wyckoff, *The Flow of Homogeneous Fluids Through Porous Media* (McGraw-Hill, New York, 1937).
 - [7] S. Whitaker, Flow in porous media I: A theoretical derivation of Darcy's law, *Transp. Porous Media* **1**, 3 (1986).
 - [8] C. W. Horton and F. T. Rogers, Jr., Convection currents in a porous medium, *J. Appl. Phys.* **16**, 367 (1945).
 - [9] D. R. Hewitt, Vigorous convection in porous media, *Proc. R. Soc. A* **476**, 20200111 (2020).
 - [10] L. Howle, R. P. Behringer, and J. Georgiadis, Visualization of convective fluid flow in a porous medium, *Nature (London)* **362**, 230 (1993).
 - [11] M. D. Shattuck, R. P. Behringer, G. A. Johnson, and J. G. Georgiadis, Onset and stability of convection in porous media: Visualization by magnetic resonance imaging, *Phys. Rev. Lett.* **75**, 1934 (1995).
 - [12] M. Weber, A. Klemm, and R. Kimmich, Rayleigh-Bénard percolation transition study of thermal convection in porous media: Numerical simulation and NMR experiments, *Phys. Rev. Lett.* **86**, 4302 (2001).
 - [13] D. R. Hewitt, J. A. Neufeld, and J. R. Lister, Ultimate regime of high Rayleigh number convection in a porous medium, *Phys. Rev. Lett.* **108**, 224503 (2012).
 - [14] B. Wen, K. W. Chang, and M. A. Hesse, Rayleigh-Darcy convection with hydrodynamic dispersion, *Phys. Rev. Fluids* **3**, 123801 (2018).
 - [15] A. Xu, B. R. Xu, and H. D. Xi, Pore-scale statistics of temperature and thermal energy dissipation rate in turbulent porous convection, *Phys. Rev. Fluids* **8**, 093504 (2023).
 - [16] H. Karani, M. Rashtbehesht, C. Huber, and R. L. Magin, Onset of fractional-order thermal convection in porous media, *Phys. Rev. E* **96**, 063105 (2017).
 - [17] C. Mezon, V. V. Mourzenko, J. F. Thovert, R. Antoine, F. Fontaine, A. Finizola, and P. M. Adler, Thermal convection in three-dimensional fractured porous media, *Phys. Rev. E* **97**, 013106 (2018).
 - [18] M. Tokita and T. Tanaka, Reversible decrease of gel-solvent friction, *Science* **253**, 1121 (1991).
 - [19] S. Kai and K. Hirakawa, Successive transitions in electrohydrodynamic instabilities of nematics, *Prog. Theor. Phys. Suppl.* **64**, 212 (1978).
 - [20] J. T. Gleeson, Charge transport measurement during turbulent electroconvection, *Phys. Rev. E* **63**, 026306 (2001).
 - [21] J. T. Gleeson, N. Gheorghiu, and E. Plaut, Electric Nusselt number characterization of electroconvection in nematic liquid crystals, *Eur. Phys. J. B* **26**, 515 (2002).
 - [22] I. Dierking, Polymer network-stabilized liquid crystals, *Adv. Mater.* **12**, 167 (2000).

- [23] S. Kai, W. Zimmermann, M. Andoh, and N. Chizumi, Local transition to turbulence in electrohydrodynamic convection, *Phys. Rev. Lett.* **64**, 1111 (1990).
- [24] To accurately determine V_c from the pattern, one method involves observing the temporal evolution of the pattern's contrast after applying step-function voltages above V_c . The voltage at which the reciprocal of the contrast growth rate reaches zero is defined as V_c . However, because this procedure requires a prolonged measurement during which the liquid-crystal sample might deteriorate, V_c was instead determined by visual observation. Although convective patterns are expected to develop simultaneously throughout the entire system, in practice, due to the inevitable inhomogeneity in the liquid crystal cell, they initially appear only in part of the observation area. Thus, V_c is defined as the voltage at which the pattern appears over approximately half of the observation area.
- [25] E. Plaut and W. Pesch, Extended weakly nonlinear theory of planar nematic convection, *Phys. Rev. E* **59**, 1747 (1999).
- [26] N. Oikawa, T. Gunji, and Y. Hidaka, Grid pattern emerging from complex dynamics of defects, *Phys. Rev. E* **101**, 062204 (2020).
- [27] S. Liu, L. Jiang, K. L. Chong, X. Zhu, Z.-H. Wan, R. Verzicco, R. J. A. M. Stevens, D. Lohse, and C. Sun, From Rayleigh-Bénard convection to porous-media convection: how porosity affects heat transfer and flow structure, *J. Fluid Mech.* **895**, A18 (2020).
- [28] M. Tokita, Transport phenomena in gel, *Gels* **2**, 17 (2016).
- [29] D. Korba and L. Li, Effects of pore scale and conjugate heat transfer on thermal convection in porous media, *J. Fluid Mech.* **944**, A28 (2022).
- [30] S. Gasow, Z. Lin, H. C. Zhang, A. V. Kuznetsov, M. Avila, and Y. Jin, Effects of pore scale on the macroscopic properties of natural convection in porous media, *J. Fluid Mech.* **891**, A25 (2020).